Eur. J. Mineral., 36, 397–409, 2024
https://doi.org/10.5194/ejm-36-397-2024

European Journal of Mineralogy
Open Access

Kenoargentotetrahedrite-(Zn), $[Ag_6]^{4+}(Cu_4Zn_2)Sb_4S_{12}\square$, a new member of the tetrahedrite group from the Yindongpo Au deposit, China

Kai Qu[1,2], Xianzhang Sima[1], Xiangping Gu[3], Weizhi Sun[4], Guang Fan[5], Zeqiang Yang[4], and Yanjuan Wang[6,7]

[1]Tianjin Center, China Geological Survey, Tianjin, 300171, China
[2]School of Earth Sciences and Engineering, Nanjing University, Nanjing, 210023, China
[3]School of Geosciences and Info-Physics, Central South University, Changsha, 410083, China
[4]No. 3 Institute of Geological and Mineral Resources Survey of Henan Geological Bureau, Xinyang, 464000, China
[5]Institute of Science and Technology Information, Beijing Research Institute of Uranium Geology, Beijing, 100029, China
[6]School of Earth Sciences and Resources, China University of Geosciences, Beijing, 100083, China
[7]Department of Geosciences, University of Padua, Padua, 35131, Italy

Correspondence: Kai Qu (qukai_tcgs@foxmail.com) and Yanjuan Wang (wangyanjuan_cugb@foxmail.com)

Received: 26 December 2023 – Revised: 22 March 2024 – Accepted: 25 March 2024 – Published: 3 May 2024

Abstract. The new mineral kenoargentotetrahedrite-(Zn), $[Ag_6]^{4+}(Cu_4Zn_2)Sb_4S_{12}\square$, was discovered at the Yindongpo Au deposit, Henan Province, China. It occurs as black metallic anhedral grains or equant crystals up to 40 µm in size. It is opaque in transmitted light and shows a greenish-grey colour in reflected light. Electron microprobe analysis for the studied material gave the empirical formula (on the basis of total cations being equal to 16 atoms per formula unit, apfu): $^{M(2)}(Ag_{3.75}Cu_{2.25})_{\Sigma 6}{}^{M(1)}[Cu_{3.90}(Zn_{1.18}Fe_{0.69}Cd_{0.26})_{\Sigma 2.13}]_{\Sigma 6.03}{}^{X(3)}(Sb_{3.69}As_{0.27})_{\Sigma 3.96}{}^{S(1)}S_{11.94}{}^{S(2)}\square$. Kenoargentotetrahedrite-(Zn) is cubic, $I\bar{4}3m$ (no. 217), with $a = 10.4624(4)$ Å, $V = 1145.23(13)$ Å^3, and $Z = 2$. The crystal structure has been refined to a final value of $R_1 = 0.0247$ on the basis of 274 independent reflections ($F_o > 4\sigma$ (F_o)) by using single-crystal X-ray diffraction data. The seven strongest X-ray powder diffraction lines (d in Å (I) (hkl)) are the following: 3.010 (100) (222), 1.844 (30) (044), 2.606 (22) (004), 1.572 (15) (226), 2.046 (9) (134), 7.35 (6) (011), and 1.909 (5) (125). Kenoargentotetrahedrite-(Zn) is isostructural with other keno-member tetrahedrites with the $[Ag_6]^{4+}$ cluster. The structure refinement result confirms the coupling between the site occupancy factor of subvalent hexasilver clusters at the $M(2)$ site and that of the vacancy at the $S(2)$ site. This relationship further substantiates the charge balance substitution mechanism of S-deficiency tetrahedrites: $6{}^{M(2)}Ag^{+} + {}^{S(2)}S^{2-} = {}^{M(2)}[Ag_6]^{4+} + {}^{S(2)}\square$.

1 Introduction

The nomenclature and classification of the tetrahedrite group was approved by the IMA CNMNC (International Mineralogical Association Commission on New Minerals, Nomenclature and Classification) in 2019 (Biagioni et al., 2020a), and the general formula can be written as follows: $^{M(2)}A_6^{M(1)}(B_4C_2)^{X(3)}D_4^{S(1)}Y_{12}^{S(2)}Z$, where A is Cu^+, Ag^+, □ (vacancy), and $[Ag_6]^{4+}$ clusters for A_6; B is Cu^+ and Ag^+; C is Zn^{2+}, Fe^{2+}, Hg^{2+}, Cd^{2+}, Mn^{2+}, Ni^{2+}, Cu^{2+}, Cu^+, In^{3+}, and Fe^{3+}; D is Sb^{3+}, As^{3+}, Bi^{3+}, and Te^{4+}; Y is S^{2-} and Se^{2-}; and Z is S^{2-}, Se^{2-}, and □ (vacancy). The tetrahedrite group is divided into 11 different series on the basis of the A, B, D, and Y constituents. There are four different min-

eral series among them in which silver predominates in the $M(2)$ or $M(1)$ crystallographic position (i.e. freibergite series, rozhdestvenskayaite series, arsenofreibergite series, and zvěstovite series). Freibergite was first reported by von Weissenbach (1831) and named by Kenngott (1853), inferring an Ag-rich tetrahedrite occurring at Freiberg, Saxony, Germany. The definition of freibergite was not clear from the very beginning, and geologists usually used it ambiguously to describe Ag-rich tetrahedrite for a long time. In fact, freibergite reports in the literature included both the recently approved tetrahedrite series (Ag < 3 apfu), the freibergite series (3 < Ag < 8 apfu), and even the rozhdestvenskayaite series (Ag > 8 apfu). Previous studies of Ag-bearing tetrahedrite-group minerals show that Ag priority is ordered at the $M(2)$ site, and the residual Ag atoms will occupy the $M(1)$ site only when Ag is in excess of 6 apfu (Kalbskopf, 1972; Johnson and Burnham, 1985; Peterson and Miller, 1986; Charnock et al., 1988).

It has been noted for over 50 years that there is a relationship between the unit-cell parameters and Ag content (Shimada and Hirowatari, 1972; Riley, 1974; Welch et al., 2018). The abnormal trend of decreasing "a" with the increasing Ag for Cu substitution in Ag-rich tetrahedrite (Ag > 4 apfu) has been explained by Rozhdestvenskaya (1993) when Ag predominantly or entirely replaced Cu at the $M(2)$ site: the $S(2)$ site became vacant, with the formation of an $[Ag_6]^{4+}$ for charge balance. Based upon this, an idealized formula as $(Ag_{4+2x}Cu_{2-2x})[(Cu, Ag)_4(Fe, Zn)_2]_{\Sigma 6}Sb_4S_{12}S_{1-x}$ $(0 < x < 1)$ for this abnormal trend was given by Moëlo et al. (2008), and it was proposed that it can be considered to belong to a specific species (freibergite) which is distinct from regular Ag-rich tetrahedrite (argentotetrahedrite). Finally, the structure feature of freibergite with vacancies at the $S(2)$ site was confirmed and clarified by Welch et al. (2018) and was renamed to kenoargentotetrahedrite-(Fe) during the establishment of the nomenclature of tetrahedrite (Biagioni et al., 2020a). $[Ag_6]^{4+}$ clusters are rare in nature, only found in Ag-rich tetrahedrite, i.e. kenoargentotetrahedrite-(Fe) (Welch et al., 2018, renamed by Biagioni et al., 2020a), kenoargentotetrahedrite-(Zn) (this study), kenoargentotennantite-(Fe) (Biagioni et al., 2020b), and kenorozhdestvenskayaite-(Fe) (Qu et al., 2023).

In this paper, the description of kenoargentotetrahedrite-(Zn) is reported, including a detailed description of the mineral paragenesis, Raman spectroscopy, chemical composition, crystal structure refinements, and crystal chemistry discussions for this extremely rare $[Ag_6]^{4+}$-cluster-containing tetrahedrite-group mineral. The new mineral, its name, and its symbol (Kattr-Zn) have been approved by the International Mineralogical Association (IMA) Commission on New Minerals, Nomenclature and Classification (CNMNC) (IMA 2020-075). The type material is deposited at the Geological Museum of China, No. 16, Yangrou Hutong, Xisi, Beijing, 100031, People's Republic of China, under catalogue number M16112.

2 Occurrences and paragenesis

The new mineral kenoargentotetrahedrite-(Zn) was discovered in the Yindongpo mine, Weishancheng ore field, Tongbai County, Nanyang, Henan Province, China (32°33′02″ N, 113°25′25″ E). The Yindongpo mine is a super-large hydrothermal Au–Ag-dominated polymetallic deposit in the Tongbai orogen, central China. The ore-forming process took place during continental collision between the Yangtze Block and the North China Block (Zhang et al., 2013). Three-stage fluid–rock interactions can be identified in the wall rock alteration, i.e. silicification, sericitization, and carbonation–chloritization (Zhang et al., 2011, 2013). The main orebodies are hosted in silicified quartz–sericite schist and/or carbonaceous quartz–sericite schist.

Kenoargentotetrahedrite-(Zn) usually occurs as anhedral grains or equant crystals up to 40 µm in size. It is closely associated with kenoargentotetrahedrite-(Fe), tetrahedrite-(Zn), sphalerite, galena, pyrite, acanthite, chalcopyrite, and quartz (Fig. 1). Kenoargentotetrahedrite-(Zn) is black in colour, and the luster is metallic. It is brittle with a conchoidal fracture. It is opaque in transmitted light and shows a greenish-grey colour in reflected light, and internal reflection is brown-red. Micro-indentation hardness (Vickers hardness number, VHN) (50 g load) was measured using a micro Vickers hardness tester with both diagonals measured for each indentation, and the values range from 288.7 to 324.1 kg mm^{-2} (mean value of four measurements: 309.7 kg mm^{-2}). The density of 5.209 g cm^{-3} was calculated based on the empirical formula and unit-cell volume refined from single-crystal XRD (X-ray diffraction) data.

3 Raman spectroscopy

The Raman spectrum was collected on a polished thin section at Tianjin Center, China Geological Survey, using a Renishaw via Raman microscope with a 532 nm laser (4 mW, 1 µm) in a measurement range of 1200–100 cm^{-1} (Fig. 2). The major Raman band of kenoargentotetrahedrite-(Zn) at 353 cm^{-1} is assigned to Sb–S stretching vibrations. The weak intensity shoulder at 346 cm^{-1} is assigned to antisymmetric stretching, which is consistent with the previous Raman spectra study of the tetrahedrite–tennantite solid solutions (Kharbish et al., 2007). The symmetric bending and antisymmetric bending modes appear as weak peaks at 314 and 282 cm^{-1}, respectively. A number of low-wavenumber bands observed at 214, 201, and 160 cm^{-1} can be described as lattice vibrations.

4 Chemical composition

The chemical composition was determined at the Beijing Research Institute of Uranium Geology with a JXA-8100 electron microprobe under operating conditions of

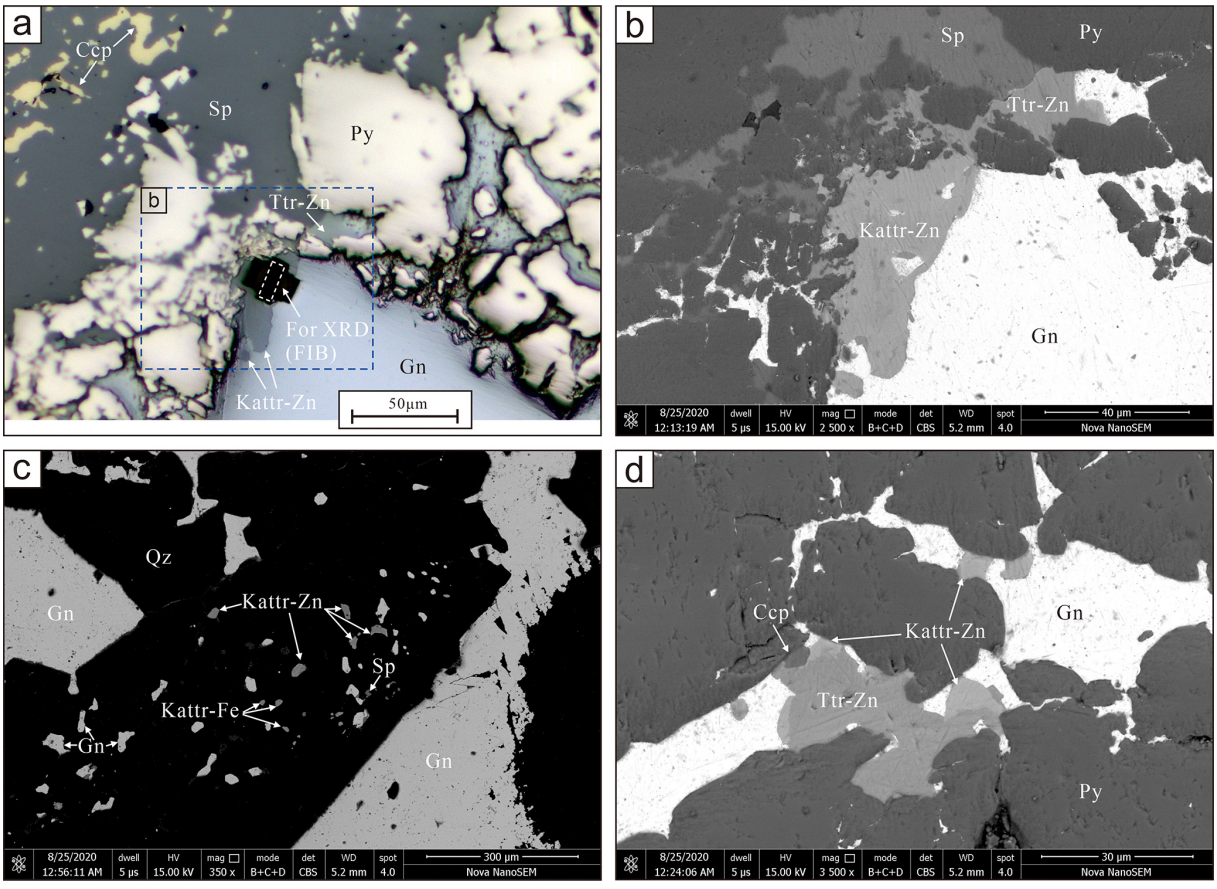

Figure 1. **(a)** Plane-polarized reflected-light images and **(b–d)** backscattered electron (BSE) images of kenoargentotetrahedrite-(Zn) and associated mineral assemblage. Kattr-Zn: kenoargentotetrahedrite-(Zn), Kattr-Fe: kenoargentotetrahedrite-(Fe), Ttr-Zn: tetrahedrite-(Zn), Sp: sphalerite, Gn: galena, Ccp: chalcopyrite, Py: pyrite, and Qz: quartz. Mineral symbols are quoted from Warr (2021).

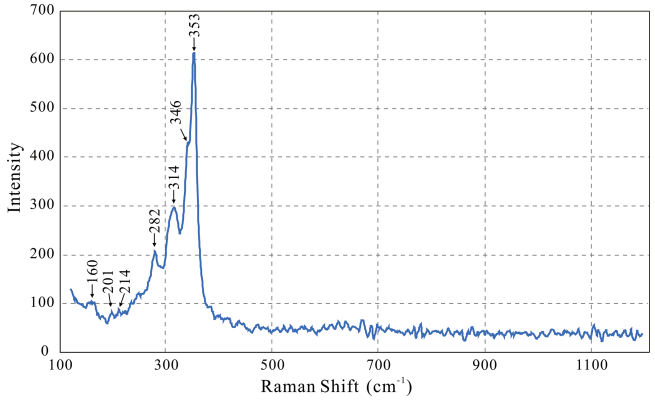

Figure 2. Raman spectrum of kenoargentotetrahedrite-(Zn).

20 kV accelerating voltage, 10 nA beam current, and 1 µm beam diameter. The standards used were pure silver (Ag), chalcopyrite (Cu, S), ZnS (Zn), pyrite (Fe), CdSe (Cd), Sb_2S_3 (Sb), and GaAs (As). The ZAF (atomic number–absorption–fluorescence) correction was applied. The average of nine electron microprobe analyses (wt %) is given in Table 1. The general formula is calculated on the basis of 16 cations per formula unit, yielding the formula of $^{M(2)}(Ag_{3.75}Cu_{2.25})_{\Sigma 6.00}{}^{M(1)}[Cu_{3.90}(Zn_{1.18}Fe_{0.69}Cd_{0.26})_{\Sigma 2.13}]_{\Sigma 6.03}{}^{X(3)}(Sb_{3.69}As_{0.27})_{\Sigma 3.96}{}^{S(1)}S^{S(2)}_{11.94}\square$, which can be simplified as (Ag, Cu)$_6$[Cu$_4$(Zn, Fe, Cd)$_2$](Sb, As)$_4$S$_{12}\square$. The ideal formula, $Ag_6(Cu_4Zn_2)Sb_4S_{12}\square$, requires 33.99 wt % Ag, 13.35 wt % Cu, 6.87 wt % Zn, 25.58 wt % Sb, and 20.21 wt % S (100 wt % total).

5 X-ray crystallography and structure refinement

The crystal for XRD analysis, with dimensions of $7 \times 6 \times 5$ µm, was extracted from the polished thin section at the Institute of Microstructure and Property of Advanced Materials, Beijing University of Technology, by using an FEI Helios NanoLab 600i dual-beam system equipped with a focused ion beam (FIB) and scanning electron microscope (SEM). Both powder and single-crystal X-ray studies of kenoargentotetrahedrite-(Zn) were carried out using a Rigaku XtaLAB Synergy diffractometer (Mo$K\alpha$ radia-

Table 1. Chemical data (wt %) for kenoargentotetrahedrite-(Zn).

%	1	2	3	4	5	6	7	8	9	Mean	SD
Ag	20.57	23.64	22.01	24.97	22.7	22.81	22.98	22.57	20.32	22.51	1.44
Cu	23.6	20.67	22.67	20.62	21.53	21.89	21.42	20.83	22.55	21.75	1.02
Zn	3.03	6.52	3.14	3.96	5.28	3.10	4.12	4.52	4.89	4.28	1.16
Fe	2.40	0.45	2.70	2.24	1.48	2.52	2.21	2.56	2.87	2.16	0.75
Cd	1.90	0.50	1.68	1.91	1.78	1.26	2.13	1.80	1.61	1.62	0.48
Sb	24.91	25.20	24.77	24.90	25.02	25.05	24.65	24.99	25.24	24.97	0.19
As	1.36	1.12	1.38	1.06	1.29	1.21	1.06	0.99	0.84	1.15	0.18
S	21.80	21.20	21.58	20.94	21.5	21.51	21.37	20.48	21.20	21.29	0.39
Total	99.57	99.30	99.93	100.60	100.58	99.35	99.94	98.74	99.52	99.73	0.61
apfu											
Ag	3.42	3.99	3.65	4.15	3.76	3.84	3.84	3.78	3.34	3.75	0.25
Cu	6.67	5.92	6.39	5.82	6.06	6.25	6.07	5.92	6.29	6.15	0.27
Zn	0.83	1.82	0.86	1.09	1.44	0.86	1.13	1.25	1.33	1.18	0.32
Fe	0.77	0.15	0.87	0.72	0.47	0.82	0.71	0.83	0.91	0.69	0.24
Cd	0.30	0.08	0.27	0.30	0.28	0.20	0.34	0.29	0.25	0.26	0.08
Sb	3.67	3.77	3.64	3.67	3.67	3.73	3.65	3.70	3.68	3.69	0.04
As	0.33	0.27	0.33	0.25	0.31	0.29	0.25	0.24	0.20	0.27	0.04
S	12.21	12.04	12.05	11.71	11.99	12.18	12.01	11.53	11.72	11.94	0.23
Total	28.21	28.04	28.05	27.71	27.99	28.18	28.01	27.53	27.72	27.94	0.23

SD: standard deviation. The metric of atoms per formula unit (apfu) was calculated on the basis of a total of 16 cations.

tion) at the School of Geosciences and Info-Physics, Central South University. The X-ray powder diffraction data were recorded using the Gandolfi technique in powder mode at 50 kV and 1 mA. The pattern was indexed on the basis of the calculated pattern based on the unit-cell parameters and the structural model determined by single-crystal X-ray diffraction using the CHEKCELL software package (Laugier and Bochu, 2000). The refined lattice parameters yielded from the powder patterns are $a = 10.4336(5)$ Å and $V = 1135.81(17)$ Å^3. The observed and indexed powder diffraction data for kenoargentotetrahedrite-(Zn) are listed in Table 2.

Single-crystal X-ray diffraction studies were performed using a Rigaku XtaLAB Synergy diffractometer equipped with a hybrid pixel array detector and Mo$K\alpha$ radiation at 50 kV and 1 mA. The intensity data were corrected for X-ray absorption using the multi-scan method, and empirical absorption correction was performed using CrysAlisPro software spherical harmonics, which was implemented in the SCALE3 ABSPACK scaling algorithm (Rigaku Oxford Diffraction, 2021). The refined unit-cell parameters are $a = 10.4624(4)$ Å, $V = 1145.23(13)$ Å^3, and space group $I\bar{4}3m$. The crystal structure was refined using the SHELX (Sheldrick, 2015) and Olex2 software packages (Dolomanov et al., 2009). In the first stage, the structure refinement was performed with the non-splitting model of the $M(2)$ site, in agreement with the literature (e.g. Wuensch, 1964; Johnson et al., 1988). The $S(1)$ and $S(2)$ sites were refined using the S neutral scattering curve: S and S vs. $\square$, respectively, while the $M(2)$, $M(1)$, and $X(3)$ sites were appropriately fixed, corresponding to the chemical compositions. Several cycles of isotropic refinement converged to $R_1 = 0.0452$, confirming the correctness of the structural model. An anisotropic structural model for all atoms converged to $R_1 = 0.031$. However, the U_{eq} of $M(2)$ (0.0339 Å^2) is relatively larger than those of other sites, suggesting its split nature, in agreement with previous works (Welch et al., 2018; Biagioni et al., 2022a, b; Sejkora et al., 2021, 2022, 2023; Wang et al., 2023b). Although the hints of splitting are not as evident as in other cases mentioned above, the studied material of kenoargentotetrahedrite-(Zn) has a mixed (Ag, Cu) occupancy at the $M(2)$ site, and the $S(2)$ site is not fully empty. In addition, the $< M(2)\ldots S(2) >$ distance (2.043 Å) is too short for the metal–sulfur bond of the partially occupied $S(2)$ site (Fig. 3a). Therefore, a splitting model would help better understand the nature of the relationship between the $[Ag_6]^{4+}$ clusters at the $M(2)$ site and the vacancy at the $S(2)$ site (see the discussion below). The following neutral scattering curves, taken from the *International Tables for Crystallography* (Wilson, 1992), were used for the splitting model: Ag vs. $\square$ at $M(2a)$, Cu vs. $\square$ at $M(2b)$, Sb vs. As at $X(3)$, S at $S(1)$, and S vs. $\square$ at $S(2)$. The sum of the site occupancy factor (s.o.f.) at $M(2a)$ and $M(2b)$ was constrained to be 1. The $M(1)$ site was appropriately fixed, corresponding to the chemical compositions. The result of the initial free refinement shows that the s.o.f. of S at the $S(2)$ site (0.43(3) apfu)

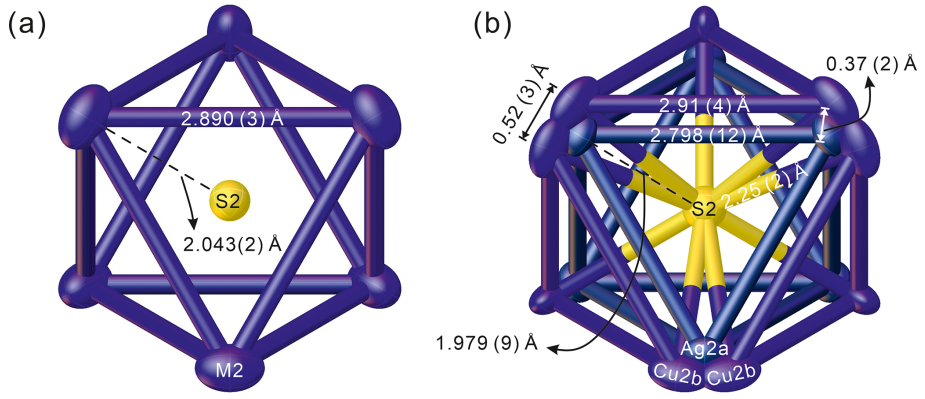

Figure 3. The $[Ag_6]^{4+}$ cluster of kenoargentotetrahedrite-(Zn): **(a)** non-split-site model and **(b)** split-site model, viewed along [111].

Table 2. X-ray powder diffraction data (d in Å) for kenoargentotetrahedrite-(Zn).

I_{meas}	d_{meas}	d_{calc}	hkl
6	**7.35**	**7.38**	**0 1 1**
1	4.25	4.26	1 1 2
3	3.670	3.689	0 2 2
100	**3.010**	**3.012**	**2 2 2**
5	2.792	2.789	1 2 3
22	**2.606**	**2.608**	**0 0 4**
5	2.456	2.459	0 3 3
3	2.224	2.225	2 3 3
9	**2.046**	**2.046**	**1 3 4**
5	**1.909**	**1.905**	**1 2 5**
30	**1.844**	**1.844**	**0 4 4**
3	1.792	1.789	3 3 4
4	1.695	1.693	2 3 5
15	**1.572**	**1.573**	**2 2 6**
1	1.505	1.506	4 4 4
1	1.327	1.325	1 5 6
1	1.305	1.304	0 0 8
1	1.228	1.230	2 2 8
1	1.212	1.213	3 4 7

The seven strongest lines are in bold.

is approximately equal to that of Cu at the two M(2b) sites (0.436(9) apfu), indicating that the occupancy of Ag at the M(2a) site should be coupled with a vacancy at the S(2) site, while the occupancy of Cu at the M(2b) site should be coupled with the occurrence of S at the S(2) site. Consequently, the s.o.f. of M(2b) was constrained to be the same as that of S(2) at the last stage. After several cycles of anisotropic refinement for all the atoms, the U_{eq} values for the M(2) site dropped to 0.0229 Å^2, and the R_1 values finally converged to 0.0247 for 274 reflections with $F_o > 4\sigma$ (F_o) and 22 refined parameters without any restraints.

Details of the data collection and the crystal structure refinement are given in Table 3. Atomic coordinates and displacement parameters are given in Tables 4 and 5, and selected distances are given in Table 6. The bond-valence sum (BVS), calculated using the bond-valence parameters of Brese and O'Keeffe (1991), is shown in Table 7. The initial structure refinement results of the non-splitting mode for the M(2) site (Tables S1–S5) are given in the Supplement.

6 Discussion

6.1 Structure description

The crystal structure of kenoargentotetrahedrite-(Zn) agrees with the general features of kenoargentotetrahedrite-(Fe) and other keno-member tetrahedrites (Welch et al., 2018; Biagioni et al., 2020b; Qu et al., 2023), with the occurrence of the $[Ag_6]^{4+}$ cluster replacing the S(2)-centred Ag_6 octahedron.

The tetrahedrally coordinated M(1) site shows an average bond distance of 2.3427(16) Å, in accordance with the values of argentotetrahedrite-(Zn), which range from 2.3386 to 2.3475 Å (Sejkora et al., 2022). On the basis of the electron microprobe data, the occupancy at the M(1) site can be given as $Cu_{0.65}Zn_{0.20}Fe_{0.15}$, neglecting minor Cd. The calculated bond distance of 2.340 Å can be compared with the observed data. The BVS of the M(1) site is 1.48 valence units (v.u.), close to the theoretical value of 1.33 v.u. The M(2) site is split into two sub-positions: the M(2a) (12e) sub-position and the M(2b) (24g) sub-position. The M(2a) sub-position has a triangular planar coordination located between two M(2b) sub-positions, with the latter having a flat trigonal pyramidal coordination symmetrically positioned on both sides of the $S(1)_2S(2)$ triangular plane. M(2a) and M(2b) are separated by 0.37(2) Å, and the distance between two neighbouring M(2b) sub-positions is 0.52(3) Å. These distances are significantly short and almost half of those reported in other tetrahedrite-group minerals characterized by a split M(2) site (e.g. 0.60–1.08 for M(2a) Å, 1.20–2.00 Å for M(2b), Makovicky et al., 2005;

Table 3. Information on structural refinement for kenoargentotetrahedrite-(Zn).

Crystal data	
General formula	$Ag_{3.37}Cu_{6.53}Zn_{1.20}Fe_{0.90}Sb_{3.70}As_{0.30}S_{12.44}$
Formula weight	1779.22
Crystal size (µm)	$7 \times 6 \times 5$
Crystal system	cubic
Space group	$I\bar{4}3m$ (no. 217)
Unit-cell dimensions	$a = 10.4624(4)$ Å
Volume	1145.23(13) Å^3
Z	2
Data collection and refinement	
Instrument	Rigaku Synergy
Radiation, wavelength, temperature	Mo$K\alpha$, 0.71073 Å, 293(2) K
$F(000)$	1609
2θ range (°)	5.50 to 56.48
Total reflections	1089
Unique reflections (all)	294
Unique reflections ($I > 4\sigma(I)$)	274
R_{int}	0.0341
R_σ	0.0328
Range of h, k, l	$-11 \le h \le 10$; $-10 \le k \le 3$; $-13 \le l \le 8$
R_1, wR_2 ($F_o > 4\sigma$ (F_o))[a]	$R_1 = 0.0247$, $wR_2 = 0.0383$
R_1, wR_2 (all data)	$R_1 = 0.0289$, $wR_2 = 0.0389$
Goodness of fit	1.111
No. of parameters, restraints	22, 0
Maximum and minimum residual peak (e Å^{-3})	0.472 (1.63 Å from M(2b))
	−0.586 (1.18 Å from M(2b))
Flack parameter[b]	−0.04(8)

[a] $w = 1/[\sigma^2(F_o^2) + (0.0097P)^2]$, where $P = (F_o^2 + 2F_c^2)/3$. [b] Flack (1983).

Table 4. Site, Wyckoff position, site occupancy factor (s.o.f.), fractional atomic coordinate, and equivalent isotropic displacement parameter (in Å^2) for kenoargentotetrahedrite-(Zn).

Site	Wyckoff	s.o.f	x/a	y/b	z/c	U_{eq}
M(2a)	12e	$Ag_{0.562(19)}$	0.1891(8)	0	0	0.0229(9)
M(2b)	24g	$Cu_{0.219(9)}$	0.214(2)	0.0175(14)	$-y$	0.0229(9)
M(1)	12d	$Cu_{0.65}Zn_{0.20}Fe_{0.15}$	1/4	1/2	0	0.0171(6)
X(3)	8c	$Sb_{0.928(19)}As_{0.072(19)}$	0.26912(6)	x	x	0.0143(4)
S(1)	24g	S	0.11839(18)	x	0.3629(2)	0.0153(6)
S(2)	2a	$S_{0.438(19)}$	0	0	0	0.027(5)

Andreasen et al., 2008; Sejkora et al., 2021; Biagioni et al., 2022a; b). An unconstrained refinement of the M(2a) and M(2b) sites was performed, resulting in $M(2a) = Ag_{0.562(19)}$ and $M(2b)^{\times 2} = Cu_{0.438(9)}$, suggesting Ag is dominant at the M(2) site. The bond distance of M(2a)–S(1), at 2.525 (7) Å, is consistent with the $<$Ag–S$>$ distance of other Ag-rich tetrahedrites, i.e. kenoargentotetrahedrite-(Fe) (2.554 Å, Welch et al., 2018) and kenorozhdestvenskayaite-(Fe) (2.550 Å, Qu et al., 2023). The distance between M(2a) and S(2) (centroid), 1.979(9) Å, is too short for the Ag–S bond, in agreement with other keno-member tetrahedrites, indicating the formation of the $[Ag_6]^{4+}$ cluster instead of the $M(2)_6S(2)$ octahedron. The observed $<M(2b)–S(2)>$ distance (2.25(2) Å) can be compared with that of flat trigonal pyramidal coordination in tetrahedrite-(Cd) (2.32(2) Å, Sejkora et al., 2023), and it is also consistent with the Cu–S distance in triangular coordination of tetrahedrite-(Hg), i.e. 2.242(4) Å for a Cu(2)–S(2) bond (Biagioni et al., 2020c). Therefore, the M(2b)–S(2) distance of the studied material can be considered reasonable for a Cu-occupied position.

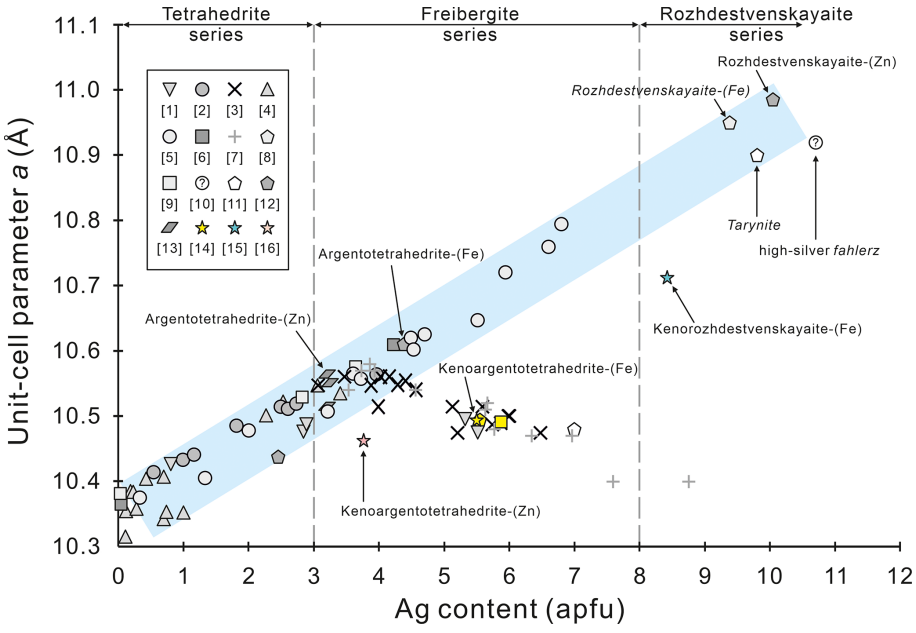

Figure 4. The relationship between the unit-cell parameter a (Å) and the Ag content (apfu) in the Ag-bearing tetrahedrite species (modified after Biagioni et al., 2020a). Taking into account the effect of the ionic radius on the a parameter, the reported Ag-bearing tetrahedrite data were selected on the basis of Ag > 0.1, As < 0.5, Cd < 0.3, and Hg < 0.1 (apfu). Further considering the existence of the keno-member tetrahedrite, the Ag content (apfu) is recalculated on the basis of 16 cations per formula unit. The pink, yellow, and blue spots are kenoargentotetrahedrite-(Zn), kenoargentotetrahedrite-(Fe), and kenorozhdestvenskayaite-(Fe), confirmed by single-crystal structure determination, respectively. References: (1) Petruk (1971), (2) Shimada and Hirowatari (1972), (3) Riley (1974), (4) Charlat and Lévy (1975), (5) Pattrick and Hall (1983), (6) Peterson and Miller (1986), (7) Balitskaya et al. (1989), (8) Li and Wang (1990), (9) Rozhdestvenskaya et al. (1993), (10) Zhdanov et al. (1992), (11) Samusikov and Gamyanin (1994), (12) Welch et al. (2018), (13) Sejkora et al. (2022), (14) Shu et al. (2022), (15) Qu et al. (2023), (16) this study.

Table 5. Anisotropic displacement parameters (in $Å^2$) for kenoargentotetrahedrite-(Zn).

Site	U_{11}	U_{22}	U_{33}	U_{23}	U_{13}	U_{12}
M(2a)	0.014(3)	0.0272(17)	U_{22}	−0.0068(18)	0	0
M(2b)	0.014(3)	0.0272(17)	U_{22}	−0.0068(18)	0	0
M(1)	0.0207(12)	0.0203(13)	0.0155(6)	U_{22}	0	0
X(3)	0.0143(4)	U_{11}	U_{11}	−0.0017(3)	U_{23}	U_{23}
S(1)	0.0144(8)	U_{11}	0.0172(15)	−0.0003(7)	U_{23}	−0.0015(9)
S(2)	0.027(5)	U_{11}	U_{11}	0	0	0

The evidence for Ag–Ag bonding in kenoargentotetrahedrite-(Zn) can be found in the $^{M(2)}$Ag–$^{M(2)}$Ag distance of 2.798(12) Å (Fig. 3b). This value compares closely with 2.85 Å of metallic silver and Ag–Ag distances reported in synthetic ternary phosphides, $Ag_6M'_6M_4P_{12}$ (e.g. $Ag_6Si_6Sn_4P_{12}$: 2.890 Å, von Schnering and Hoenle, 1979; $Ag_6Ge_{10}P_{12}$: 2.838 Å, Nuss et al., 2017), and other keno-member tetrahedrites (i.e. kenoargentotetrahedrite-(Fe), Welch et al., 2018; kenorozhdestvenskayaite-(Fe), Qu et al., 2023), which is markedly different from the observed Ag–Ag length of argentotetrahedrite-(Zn) (3.195 to 3.250 Å, Sejkora et al., 2022). As a result, the volumes of the $[Ag_6]^{4+}$ cluster in the keno-member freibergites (10.33–10.81 $Å^3$) are approximately 50 % smaller than the volumes of the $M(2)_6S(2)$ octahedron (15.37–16.18 $Å^3$) in non-keno-member ones (Table 8), which is also consistent with the observation that the $M(2)\ldots$centroid distance (mean: 1.99 Å) of keno-member freibergites is significantly shorter than the $M(2)$–$S(2)$ bond length of non-keno-member freibergites (mean: 2.28 Å). The BVS result of $M(2)$ (0.79 v.u.) is consistent with the theoretically calculated BVS (0.81 v.u.), further confirming the presence of the $[Ag_6]^{4+}$ cluster for the studied material (Table 7).

The $X(3)$ site has an average bond distance of 2.436(3) Å with a BVS of 3.03 v.u., which is consistent with the theoreti-

Table 6. Selected bond distances (Å) and polyhedral volumes ($Å^3$) for kenoargentotetrahedrite-(Zn).

$M(2a)$–$S(1)^{\times 2}$	2.525(7)	$M(1)$–$S(1)^{\times 4}$	2.3427(16)
$-S(2)^{\times 1}$	– *	$[M(1)S(1)_4]$ tel. vol.	6.59
$[Ag_6]^{4+}$ cluster oct. vol.	10.326	$X(3)$–$S(1)^{\times 3}$	2.436(3)
$M(2b)$–$S(1)^{\times 2}$	2.360(16)	$[X(3)S(1)_3]$ tri. pyramid vol.	2.37
$-S(2)^{\times 1}$	2.25(2)		

* $M(2)$... centroid distance for kenoargentotetrahedrite-(Zn) = 1.979(9) Å. Ag–Ag = 2.798(12) Å.

cal value of mixed-occupied trivalent cations. The results can also be compared to values reported in other freibergite series species (for instance, 2.438 Å, Welch et al., 2018; 2.436 Å, Shu et al., 2022; 2.397 to 2.438 Å, Sejkora et al., 2022).

The $S(1)$ site is 4-fold coordinated, being bonded to two $M(1)$ sites, one $M(2)$ site, and one $X(3)$ site. The BVS of $S(1)$ is 2.07 v.u., in agreement with the occurrence of S^{2-}. On the contrary, the $[\square_{0.562}S_{0.438(19)}]$ occupancy of $^{S(2)}Z$ is consistent with its lower BVS result (0.90 v.u.), indicating the vacancy is dominant at the $S(2)$ site. Interestingly, the s.o.f of S at the $S(2)$ site is approximately equal to that of Cu at the splitting $M(2)$ site. A similar phenomenon has been observed in other keno-member tetrahedrites, i.e. kenorozhdestvenskayaite-(Fe), $[Ag_{0.90(3)}Cu_{0.10(3)}]$ at the $M(2)$ site coupled with $[\square_{0.86}S_{0.14(11)}]$ at the $S(2)$ site (Qu et al., 2023). This coupling between the presence of subvalent hexasilver clusters at the $M(2)$ site and that of the S deficiency at the $S(2)$ site further substantiates the following charge balance substitution mechanism of keno-member tetrahedrite-group minerals: $6^{M(2)}Ag^{+} + {}^{S(2)}S^{2-} = {}^{M(2)}[Ag_6]^{4+} + {}^{S(2)}\square$ (Rozhdestvenskaya et al., 1993; Welch et al., 2018; Qu et al., 2023). On the basis of this correlation, the general structural formula for the Ag-rich keno-member tetrahedrite could be described as the following: $[(Ag_6)_x^{4+}(Cu_6)_{1-x}^{6+}]_6M(1)_6X3)_4S(1)_{12}[\square_x S(2)_{1-x}]$ $(0.5 < x \leq 1)$. Taking into account that it is also probable that both the $[Ag_6]^{4+}$ cluster and Ag_6S octahedron occur in some purely silver-occupied $M(2)$ site keno-member tetrahedrites, the crystal chemical investigation of more samples, especially the materials with full site occupancy by Ag at the $M(2)$ site, would be useful in gaining a better understanding of this coupling behaviour between the S deficiency and the $[Ag_6]^{4+}$ cluster formation.

6.2 Relationship between Ag content and unit-cell parameters

The study of relationships between Ag content and unit-cell parameters started at the beginning of the 1970s. Early studies indicated that the unit-cell parameters of Ag-bearing tetrahedrite increase in a positive linear trend with silver content (up to 4 Ag apfu) but decrease with extending silver substitution (Shimada and Hirowatari, 1972; Riley, 1974; Charlat and Lévy, 1975; Pattrick and Hall, 1983; Samusikov et al., 1988; Balitskaya et al., 1989; Welch et al., 2018). Biagioni et al. (2020a) made an up-to-date historical synopsis review of previous studies on this issue. In order to reduce the influence of different cation radii (for instance, As, Cd, and Hg) that can cause slight deviations between the chemical composition and the unit-cell parameter trend, we optimized the selection of reported data and updated some new, important data from the published Ag-bearing tetrahedrite data that include both chemical data and unit-cell parameters (Fig. 4). It clearly shows that the recently approved kenoargentotetrahedrite-(Zn) and kenorozhdestvenskayaite-(Fe) are not on the trend line of decreasing the unit-cell parameter with increasing Ag content (Ag > 4 apfu). This reminds us that in addition to the Ag–Cu content ratio, there must be other factors that restrict the formation of silver clusters in Ag-bearing tetrahedrite, e.g. sulfur fugacity (Sack et al., 2022; Qu et al., 2023) or the radius of the cation at $X(3)$, which could play a crucial role in promoting the formation of silver clusters in Ag-rich tetrahedrites (Nuss et al., 2017). It should be noted that the unit-cell parameter of sample no. 12 with $a = 10.40$ Å (and 8.75 Ag apfu) given by Balitskaya et al. (1989) is far away from that of chemically similar kenorozhdestvenskayaite-(Fe) ($a = 10.7119$, 8.41 Ag apfu, Qu et al., 2023). Since this result is doubtful, we strongly suggest excluding at least these data in further research on the relationships between chemistry and unit-cell parameters of Ag-bearing tetrahedrite. In addition, Li and Wang (1990) reported several Ag-rich tetrahedrite species from the Dachang ore field, Guangxi, China. The average result of nine electron microprobe analyses for three different samples from the Lame no. 11 orebody yielded 48.57 % Ag, 1.31 % Cu, 23.26 % Sb, 0.02 % As, 0.06 % Bi, 0.53 % Pb, 5.94 % Fe, 0.23 % Zn, 0.03 % Mn, 0.03 % Sn, and 19.98 % S, for a total of 99.96 %. The empirical formula is recalculated on the basis of 16 cations per formula unit, yielding $Ag_6(Ag_{3.29}Cu_{0.43}Fe_{2.19}Zn_{0.07}Pb_{0.05}Mn_{0.01})_{\Sigma 6.04}(Sb_{3.94}As_{0.01}Bi_{0.01}Sn_{0.01})_{\Sigma 3.96}S_{12.85}$, which corresponds to the ideal formula, $Ag_6(Ag_4Fe_2)Sb_4S_{13}$. The seven strongest X-ray powder diffraction lines (d in Å (I) (hkl)) are the following: 3.16 (100) (222), 1.934 (70) (044), 2.740 (50) (004), 1.648 (40) (226), 2.585 (30) (114), 2.000 (30) (125), and 7.74 (20) (110). The unit-cell parameter, $a = 10.950 \pm 0.009$ Å, is similar to that of rozhdestvenskayaite-(Zn) (10.9845 Å,

Table 7. Bond-valence sum (BVS) analysis for kenoargentotetrahedrite-(Zn).

Site	$M(2)$	$M(1)$	$X(3)$	Σanions	Theoretical
$S(1)$	$0.32^{\times 2\downarrow}$	$0.37^{\times 4\downarrow \times 2\rightarrow}$	$1.01^{\times 3\downarrow}$	2.07	2.00
$S(2)$	$0.15^{\times 6\rightarrow}$			0.90	0.88
Σcations	0.79	1.48	3.03		
Theoretical	$0.81^{\dagger}$	1.33	3.00		

Bond-valence sums were calculated with the site-occupancy factors given in Table 4. Calculations were done using the equation and constants of Brown (1977), $S = \exp[(R_0 - d_0)/b]$. Superscripts indicate the number of equivalent bonds involving cations and anions. The theoretical bond valence of $M(2)$, $M(1)$, and $S(2)$ is calculated on the basis of $0.562[Ag_6]^{4+} + 0.438(Cu_6)^{6+}$, $(2/3Me^{+} + 1/3Me^{2+})$, and $0.438S^{2-}$, respectively.

Table 8. Comparative characteristics of kenoargentotetrahedrite-(Zn), kenoargentotetrahedrite-(Fe), and argentotetrahedrite-(Zn).

	Kenoargentotetrahedrite-(Zn)	Kenoargentotetrahedrite-(Fe)[a]	Argentotetrahedrite-(Zn)[b]
Ideal formula	$Ag_6(Cu_4Zn_2)Sb_4S_{12}\square$	$Ag_6(Cu_4Fe_2)Sb_4S_{12}\square$	$Ag_6(Cu_4Zn_2)Sb_4S_{13}$
$^{M(2)}A$	$[Ag_6]^{4+}$	$[Ag_6]^{4+}$	$(Ag_6)^{6+}$
$^{M(1)}C$	Zn	Fe	Zn
$^{S(2)}Z$	$\square$	$\square$	S
Ag–Ag distance(Å)	2.789	2.84	3.195 to 3.250
$M(2)\ldots$centroid (S2) distance (Å)	1.979	2.009	2.259–2.298
$[Ag_6]^{4+}$ cluster or $M(2)_6S(2)$ vol. (Å^3)	10.33	10.81	15.37–16.18
a(Å)	10.4624(4)	10.4930(4)	10.5155–10.5663
V(Å^3)	1145.23(13)	1155.31(8)	1162.8–1179.7

[a] Kenoargentotetrahedrite-(Fe) named as *freibergite* in Welch et al. (2018), renamed by Biagioni et al. (2020a). [b] Sejkora et al. (2022).

Welch et al., 2018) and significantly larger than that of kenorozhdestvenskayaite-(Fe) (10.7119 Å, Qu et al., 2023), corresponding to a potential new rozhdestvenskayaite series species, *rozhdestvenskayaite-(Fe)*, characterized as $8 < Ag < 10$ apfu, $0.5 < {}^{S(2)}S < 1.0$, and Fe > Zn at the $M(1)$ site.

6.3 Relationship between Ag content and equivalent isotropic displacement parameters (U_{eq}) of the $M(2)$ site

The relatively large U_{eq} value of the $M(2)$ site in tetrahedrite-group minerals has been well known for decades. The $M(2)$ site of Ag-bearing tetrahedrite has strongly anisotropic displacement ellipsoids, as previously noted by Kalbskopf (1972). Johnson and Burnham (1985) proposed that this behaviour is better explained as thermal motion rather than splitting the $M(2)$ site into two flat pyramidal sub-sites positioned symmetrically above and below the $S(1)$–$S(2)$–$S(1)$ plane triangle. On account of a relatively strong residual in the ΔF maps, Makovicky et al. (2005) successfully introduced a split $M(2)$ position for a Cu-rich tennantite, and, as a result, a significant drop in all R values has been observed. With the approval of the tetrahedrite-group nomenclature, more and more new tetrahedrite species have been discovered all around the world in the past 5 years. In certain new mineral species, the splitting model has effectively reduced the U_{eq} of the $M(2)$ site and further decreased the R_1 value (Welch et al., 2018; Biagioni et al., 2022a, b; Sejkora et al., 2021, 2022, 2023; Wang et al., 2023b). In the splitting model, the $M(2)$ site is split into two sub-positions, $M(2a)$ at $(x, 0, 0)$ and $M(2b)$ at $(x, y, -y)$ (Andreasen et al., 2008). The $M(2a)$ sub-position has triangular planar coordination, whereas the $M(2b)$ sub-position has two flat trigonal pyramids symmetrically situated out of the $S(1)_2S(2)$ plane. The $M(2a)$ sub-position is between two $M(2b)$ sub-positions, and their axes of elongation are approximately along a line connecting two $M(2b)$ sub-positions (Makovicky et al., 2005). The sum of the site occupancy factors at the two split positions, $M(2a)$ and $M(2b)$, was generally constrained to the full occupancy (Sejkora et al., 2022; Biagioni et al., 2022a).

Kalbskopf (1972) first suggested that silver preferentially occurs at the 3-fold-coordinated $M(2)$ site and may be positionally disordered between two sites on either side of the coordination plane. Through the statistics of the recently described tetrahedrite mineral species (Table 9), indeed, as the silver content increases, the U_{eq} values of $M(2)$ show a positive correlation and increasing trend. Peterson and Miller (1986) found that although the apparent thermal motions of the atoms at the $M(2)$ site are increasing with increased Ag content, the highest anisotropy occurs in the Ag-barren tetrahedrite structure. Thus, the Ag content may not be the only limiting factor in the effect of the thermal dis-

Table 9. U_{eq} of the $M(2)$ comparison of recently described tetrahedrite-group minerals.

Mineral	Ideal formula	$M(2)$ site	s.o.f.	U_{eq}	Reference
Non-splitting mode of the $M(2)$ site					
Kenoargentotetrahedrite-(Zn)	$[Ag_6]^{4+}(Cu_4Zn_2)Sb_4S_{12}\square$	$M(2)$	$Ag_{0.63}Cu_{0.37}$	0.0339(6)	(1)
Kenoargentotetrahedrite-(Fe)	$[Ag_6]^{4+}(Cu_4Fe_2)Sb_4S_{12}\square$	$M(2)$	$Ag_{0.88}Cu_{0.12}$	0.0340(4)	(2)
		$M(2)$	$Ag_{0.95}Cu_{0.05}$	0.0278(2)	(3)
Kenorozhdestvenskayaite-(Fe)	$[Ag_6]^{4+}(Ag_4Fe_2)Sb_4S_{12}\square$	$M(2)$	$Ag_{0.90}Cu_{0.10}$	0.0464(11)	(4)
Argentotetrahedrite-(Cd)	$Ag_6(Cu_4Cd_2)Sb_4S_{13}$	$M(2)$	$Ag_{0.55}Cu_{0.45}$	0.0851(8)	(5)
Argentotetrahedrite-(Hg)	$Ag_6(Cu_4Hg_2)Sb_4S_{13}$	$M(2)$	$Ag_{0.565}Cu_{0.435}$	0.0727(11)	(6)
Argentotetrahedrite-(Fe)	$Ag_6(Cu_4Fe_2)Sb_4S_{13}$	$M(2)$	$Ag_{0.70}Cu_{0.30}$	0.0711(7)	(2)
Tetrahedrite-(Fe)	$Cu_6(Cu_4Fe_2)Sb_4S_{13}$	$M(2)$	$Cu_{0.57}Ag_{0.43}$	0.0604(7)	(2)
Tetrahedrite-(Hg)	$Cu_6(Cu_4Hg_2)Sb_4S_{13}$	$M(2)$	$Cu_{1.00}$	0.0547(11)	(7)
Tetrahedrite-(Ni)	$Cu_6(Cu_4Ni_2)Sb_4S_{13}$	$M(2)$	$Cu_{1.00}$	0.062(2)	(8)
Splitting mode of the $M(2)$ site					
Kenoargentotetrahedrite-(Zn)	$[Ag_6]^{4+}(Cu_4Zn_2)Sb_4S_{12}\square$	$M(2a)$	$Ag_{0.562}$	0.0229(9)	(1)
		$M(2b)^{\times 2}$	$Cu_{0.438}$	0.0229(9)	
Rozhdestvenskayaite-(Zn)	$Ag_6(Ag_4Zn_2)Sb_4S_{13}$	$M(2a)$	$Ag_{0.49}$	0.050(1)	(2)
		$M(2b)^{\times 2}$	$Ag_{0.51}$	0.049(1)	
Zvěstovite-(Zn)	$Ag_6(Ag_4Zn_2)As_4S_{13}$	$M(2a)$	$Ag_{0.53}$	0.048(9)	(9)
		$M(2b)^{\times 2}$	$Ag_{0.47}$	0.052(10)	
Argentotetrahedrite-(Zn)	$Ag_6(Cu_4Zn_2)Sb_4S_{13}$	$M(2a)$	$Ag_{0.52}$	0.039(4)	(10)
		$M(2b)^{\times 2}$	$Cu_{0.48}$	0.039(4)	
		$M(2a)$	$Ag_{0.54}$	0.042(3)	(10)
		$M(2b)^{\times 2}$	$Cu_{0.46}$	0.042(3)	
		$M(2a)$	$Ag_{0.67}$	0.057(5)	(10)
		$M(2b)^{\times 2}$	$Cu_{0.33}$	0.057(5)	
Tennantite-(Hg)	$Cu_6(Cu_4Hg_2)As_4S_{13}$	$M(2a)$	$Cu_{0.81}$	0.040(4)	(11)
		$M(2b)^{\times 2}$	$Ag_{0.19}$	0.040(4)	
Tennantite-(Cu)	$Cu_6(Cu_4Cu_2)As_4S_{13}$	$M(2a)$	$Cu_{0.67}$	0.034(2)	(12)
		$M(2b)^{\times 2}$	$Cu_{0.33}$	0.034(2)	
Tennantite-(Cd)	$Cu_6(Cu_4Cd_2)As_4S_{13}$	$M(2a)$	$Cu_{0.84}$	0.0380(7)	(13)
		$M(2b)^{\times 2}$	$Cu_{0.16}$	0.0380(7)	
Tennantite-(Ni)	$Cu_6(Cu_4Ni_2)As_4S_{13}$	$M(2a)$	$Cu_{0.69}$	0.041(3)	(14)
		$M(2b)^{\times 2}$	$Cu_{0.31}$	0.041(3)	
Tetrahedrite-(Cd)	$Cu_6(Cu_4Cd_2)Sb_4S_{13}$	$M(2a)$	$Cu_{0.63}$	0.036(10)	(15)
		$M(2b)^{\times 2}$	$Cu_{0.37}$	0.036(10)	

References: (1) this study, (2) Welch et al. (2018), (3) Shu et al. (2022), (4) Qu et al. (2023), (5) Mikuš et al. (2023), (6) Wu et al. (2022), (7) Biagioni et al. (2020c), (8) Wang et al. (2023a), (9) Sejkora et al. (2021), (10) Sejkora et al. (2022), (11) Biagioni et al. (2021), (12) Biagioni et al. (2022), (13) Biagioni et al. (2022b), (14) Wang et al. (2023b), (15) Sejkora et al. (2023).

placement parameters at the $M(2)$ position for tetrahedrite-group minerals. The role of the Fe content at the $M(1)$ site and the Sb–As ratio at the $X(3)$ site in affecting the degree of splitting of $M(2)$ has been confirmed by Rietveld refinement of neutron powder diffraction data (Andreasen et al., 2008). Nevertheless, the positive correlation trend of the U_{eq} values of $M(2)$ with the increasing Ag content would not be masked by the relatively insignificant effect. In contrast, the U_{eq} values of the $M(2)$ in $[Ag_6]^{4+}$ cluster-containing tetrahedrites have shown a cliff-like decrease compared to the normal Ag-rich tetrahedrite-group minerals (Table 9). Peterson and Miller (1986) noted that there is a linear relationship between the temperature factor of the $S(2)$ site and the Ag per formula unit, and the U_{eq} value of the $S(2)$ site is generally coupled with that of the $M(2)$ site. They suggested that the high apparent thermal motion of the $S(2)$ site might be attributed to the site being only partially occupied. The authors also noted that, despite the possibility of some vacancy at the $S(2)$ site, the large deficiency necessary to explain the high thermal parameter is greater than what the chemical component permits. It is worth noting that at that time, the nature of the vacancy occupancy at the $S(2)$ site in the tetrahedrite structure had not been totally understood. Therefore, they predict that the thermal motion of $S(2)$ and $M(2)$ will increase with the increase in vacancies at the $S(2)$ site. However, more and more observation results from the keno-member tetrahedrites show that $M(2)$ position silver clusters, along with the vacancy of the $S(2)$ site, can significantly reduce their U_{eq} values. Although it is expected that the formation of the $[Ag_6]^{4+}$ cluster probably plays an important role in this behaviour, there is room for a great deal more research to highlight this effect. The further investigations not only will promote and extend the understanding of the special structure features of tetrahedrite-group minerals for mineralogists but also will provide new insights for the material sciences community.

7 Conclusions

The description of this extremely rare keno-member tetrahedrite-group mineral provides new insights into the crystal chemical complexity of these common sulfosalts in hydrothermal ore deposits. On the one hand, this study confirms the coupling between the presence of the subvalent hexasilver cluster at the $M(2)$ site and that of the vacancy at the $S(2)$ site, further substantiating the charge balance substitution mechanism of S-deficiency tetrahedrites. On the other hand, it is a good case for indicating the necessity and practical meaning of splitting the $M(2)$ site in the tetrahedrite-group minerals.

Data availability. The Crystallographic Information File data of the splitting model and non-splitting mode for kenoargentotetrahedrite-(Zn) are available in the Supplement.

Supplement. The supplement related to this article is available online at: https://doi.org/10.5194/ejm-36-397-2024-supplement.

Author contributions. KQ and YW wrote the manuscript. KQ and YW carried out the scanning electron microscope (SEM) and Raman spectroscopy studies. XG, YW, and KQ carried out single-crystal X-ray diffraction and structural refinement. YW and GF conducted the microprobe analyses. XS, WS, and ZY collected the specimens and geological background information.

Competing interests. The contact author has declared that none of the authors has any competing interests.

Disclaimer. Publisher's note: Copernicus Publications remains neutral with regard to jurisdictional claims made in the text, published maps, institutional affiliations, or any other geographical representation in this paper. While Copernicus Publications makes every effort to include appropriate place names, the final responsibility lies with the authors.

Special issue statement. This article is part of the special issue "New minerals: EJM support". It is not associated with a conference.

Acknowledgements. The helpful comments from Yves Moëlo, an anonymous reviewer, and Associate Editor Cristian Biagioni are greatly appreciated. Their valuable and insightful comments have significantly improved the paper. The authors acknowledge Zengqian Hou, Pei Ni, Daming Wang, and Chao Tang for their precious help and kind advice in discovering the new mineral species. Lijuan Ye is thanked for helping with the Raman spectroscopy collection.

Financial support. For this research, Kai Qu was supported by the China Geological Survey (grant nos. DD20190121 and DD20190813). Weizhi Sun, Zeqiang Yang, Kai Qu, and Xianzhang Sima received financial support from the geological exploration project of the Henan Geological and Mineral Exploration and Development Bureau (grant no. Yudikuang202205); Xiangping Gu received support from the National Natural Science Foundation of China (NSFC) (grant no. 42072054). Yanjuan Wang and Kai Qu received support from the Chinese Scholarship Council (CSC) (grant nos. 202106400047 and 202108575009).

Review statement. This paper was edited by Cristian Biagioni and reviewed by Yves Moëlo and one anonymous referee.

References

Andreasen, J. W., Makovicky, E., Lebech, B., and Møller, S. K.: The role of iron in tetrahedrite and tennantite determined by Rietveld refinement of neutron powder diffraction data, Phys. Chem. Miner., 35, 447–454, 2008.

Balitskaya, O. V., Mozgova, N. N., Borodaev, Y. S., Efimova, A. V., and Tsepin, A. I.: Evolution of the unit-cell parameter of fahlores with their silver content, Izv. Akad. Nauk Kaz. SSR, Ser. Geol., 9, 112–120, 1989 (in Russian).

Biagioni, C., George, L. L., Cook, N. J., Makovicky, E., Moëlo, Y., Pasero, M., Sejkora, J., Stanley, C. J., Welch, M. D., and Bosi, F.: The tetrahedrite group: Nomenclature and classification, Am. Min., 105, 109–122, 2020a.

Biagioni, C., Sejkora, J., Moëlo, Y., Makovicky, E., Pasero, M., and Dolníček, Z.: Kenoargentotennantite-(Fe), IMA 2020-062, in: CNMNC Newsletter 58, Eur. J. Mineral., 32, 645–651, 2020b.

Biagioni, C., Sejkora, J., Musetti, S., Velebil, D., and Pasero, M.: Tetrahedrite-(Hg), a new "old" member of the tetrahedrite group, Mineral. Mag., 84, 584–592, 2020c.

Biagioni, C., Sejkora, J., Raber, T., Roth, P., Moëlo, Y., Dolníček, Z., and Pasero, M.: Tennantite-(Hg), $Cu_6(Cu_4Hg_2)As_4S_{13}$, a new tetrahedrite-group mineral from the Lengenbach quarry, Binn, Switzerland, Mineral. Mag., 85, 744–751, 2021.

Biagioni, C., Sejkora, J., Moëlo, Y., Marcoux, E., Mauro, D., and Dolníček, Z.: Tennantite-(Cu), $Cu_{12}As_4S_{13}$, from Layo, Arequipa Department, Peru: a new addition to the tetrahedrite-group minerals, Mineral. Mag., 86, 331–339, 2022a.

Biagioni, C., Kasatkin, A., Sejkora, J., Nestola, F., and Škoda, R.: Tennantite-(Cd), $Cu_6(Cu_4Cd_2)As_4S_{13}$, from the Berenguela mining district, Bolivia: The first Cd-member of the tetrahedrite group, Mineral. Mag., 86, 834–840, 2022b.

Brese, N. E. and O'Keeffe, M.: Bond-valence parameters for solids, Acta Crystallogr., B47, 192–197, 1991.

Brown, I. D.: Predicting bond lengths in inorganic crystals, Acta Crystallogr., B33, 1305–1310, 1977.

Charlat, M. and Lévy, C.: Influence des principales substitutions sur le paramètre cristallin dans la série tennantite-tétraédrite, Bull. Soc. Fr. Mineral. Cristallogr., 98, 152–158, 1975.

Charnock, J. M., Garner, C. D., Pattrick, R. A. D., and Vaughan, D. J.: Investigation into the nature of copper and silver sites in argentian tetrahedrites using EXAFS spectroscopy, Phys. Chem. Miner., 15, 296–299, 1988.

Dolomanov, O. V., Bourhis, L. J., Gildea, R. J, Howard, J. A. K., and Puschmann, H.: OLEX2: A complete structure solution, refinement and analysis program, J. Appl. Crystallogr., 42, 339–341, 2009.

Flack H. D.: On enantiomorph-polarity estimation, Acta Crystallogr., Sect. A: Found. Crystallogr., 39, 876–881, 1983.

Johnson, M. L. and Burnham, C. W.: Crystal structure refinement of an arsenic-bearing argentian tetrahedrite, Am. Min., 70, 165–170, 1985.

Johnson, N. E., Craig, J. R., and Rimstidt, J. D.: Crystal chemistry of tetrahedrite, Am. Min., 73, 389–397, 1988.

Kalbskopf, R.: Strukturverfeinerung des Freibergits, Tschermaks Mineral. Petrogr. Mitt., 18, 147–155, 1972.

Kenngott, A.: Das Mohs'sche Mineralsystem, dem gegenwärtigen Standpuncte der Wissenschaft gemäss bearbeitet, Gerol & Sohn, Wien, 164 pp., 1853.

Kharbish, S., Libowitzky, E., and Beran., A.: The effect of As-Sb substitution in the Raman spectra of tetrahedrite-tennantite and pyrargyrite-proustite solid solutions, Eur. J. Mineral., 19, 567–574, 2007.

Laugier, J., and Bochu, B.: CHECKCELL: a Software Performing Automatic Cell/Space Group Determination, Collaborative Computational Project, Number 14 (CCP14), Laboratory of Materials and Phyisical Engineering, School of Physics, University of Grenoble, France, 2000.

Li, X. L. and Wang, G. X.: Studies of the tetrahedrite-group minerals from Dachang ore field, Guangxi, China, Acta Min. Sin., 10, 119–126, 1990 (in Chinese with English abstract).

Makovicky, E., Karanovicì, L., Poleti, D., Balić-Žunić, T., and Paar, W. H.: Crystal structure of copper-rich unsubstituted tennantite, $Cu_{12.5}As_4S_{13}$, Can. Mineral., 43, 679–688, 2005.

Mikuš, T., Vlasáč, J., Majzlan, J., Sejkora, J., Steciuk, G., Plášil, J., Rößler, C., and Matthes, C.: Argentotetrahedrite-(Cd), $Ag_6(Cu_4Cd_2)Sb_4S_{13}$, a new member of the tetrahedrite group from Rudno nad Hronom, Slovakia, Mineral. Mag., 87, 262–270, 2023.

Moëlo, Y., Makovicky, E., Mozgova, N. N., Jambor, J. L., Cook, N., Pring, A., Paar, W. H., Nickel, E. H., Graeser, S., Karup-Møller, S., Žunic, T. B., Mumme, W. G., Vurro, F., Topa, D., Bindi, L., Bente, K., and Shimizu, M.: Sulfosalt systematics: a review. Report of the sulfosalt sub-committee of the IMA Commission on Ore Mineralogy, Eur. J. Mineral., 20, 7–46, 2008.

Nuss, J., Wedig, U., Xie, W., Yordanov, P., Bruin, J., Hübner, R., Weidenkaff, A., and Takagi, H.: Phosphide–tetrahedrite $Ag_6Ge_{10}P_{12}$: thermoelectric performance of a long-forgotten silver-cluster compound, Chem. Mater., 29, 6956–6965, 2017.

Pattrick, R. A. D. and Hall, A. J.: Silver substitution into synthetic zinc, cadmium, and iron tetrahedrites, Mineral. Mag., 47, 441–451, 1983.

Peterson, R. C. and Miller, I.: Crystal structure and cation distribution in freibergite and tetrahedrite, Mineral. Mag., 50, 717–721, 1986.

Petruk, W. and staff.: Characteristics of the sulphides, Can. Mineral., 11, 196–231, 1971.

Qu, K., Sun, W., Nestola, F., Gu, X., Yang, Z., Sima, X., Tang, C., Fan, G., and Wang, Y.: Kenorozhdestvenskayaite-(Fe), $Ag_6(Ag_4Fe_2)Sb_4S_{12}\square$: A new tetrahedrite group mineral containing a natural $[Ag_6]^{4+}$ cluster and its relationship to the synthetic ternary phosphide $(Ag_6M_4P_{12})M'_6$, Am. Min., 1–28, https://doi.org/10.2138/am-2023-9074, 2023.

Rigaku Oxford Diffraction: CrysAlisPro Software system, version 1.171.41.96a, Rigaku Corporation, 2021.

Riley, J. F.: The tetrahedrite–freibergite series, with reference to the Mount Isa Pb–Zn–Ag orebody, Miner. Deposita, 9, 117–124, 1974.

Rozhdestvenskaya, I. V., Zayakina, N. V., and Samusikov, V. P.: Crystal structure features of minerals from a series of tetrahedrite-freibergite, Mineralogiceskij Zhurnal., 15, 9–17, 1993 (in Russian).

Sack, R. O., Lyubimtseva, N. G., Bortnikov, N. S., Anikina, E. Y., and Borisovsky, S. E.: Sulfur vacancies in fahlores from the Ag-Pb–Zn Mangazeyskoye ore deposit (Sakha, Russia), Contrib. Mineral. Petrol., 177, 82, 2022.

Samusikov, V. P., Zayakina, N. V., and Leskova, N. V.: Relation between unit cell of fahlores and Ag-concentration, Doklady Akademii Nauk USSR, 299, 468–471, 1988 (in Russian).

Samusikov, V. P. and Gamyanin, G. N.: Nomenclature of mineral species of Cu-Ag isomorphous tetrahedrite, 16th IMA General Meeting, Pisa, Italy, 4–9 September 1994, 363–364, 1994.

Sejkora, J., Biagioni, C., Vrtiška, L., and Moëlo, Y.: Zvěstovite-(Zn), $Ag_6(Ag_4Zn_2)As_4S_{13}$, a new tetrahedrite-group mineral from Zvěstov, Czech Republic, Mineral. Mag., 85, 716–724, 2021.

Sejkora, J., Biagioni, C., Števko, M., Raber, T., Roth, P., and Vrtiška, L.: Argentotetrahedrite-(Zn), $Ag_6(Cu_4Zn_2)Sb_4S_{13}$, a new member of the tetrahedrite group. Mineral. Mag., 86, 319–330, 2022.

Sejkora, J., Biagioni, C., Škácha, P., Musetti, S., Kasatkin, A. V., and Nestola, F.: Tetrahedrite-(Cd), $Cu_6(Cu_4Cd_2)Sb_4S_{13}$, from Radětice near Příbram, Czech Republic: the new Cd member of the tetrahedrite group, Eur. J. Mineral., 35, 897–907, 2023.

Sheldrick, G. M.: Crystal structure refinement with SHELXL, Acta Crystallogr., C71, 3–8, 2015.

Shimada, N. and Hirowatari, F.: Argentian tetrahedrites from the Taishu-Shigekuma mine, Tsushima Island, Japan, Mineral. J., 1, 77–87, 1972.

Shu, Z., Shen, C., Lu, A., and Gu, X.: Chemical Composition and Crystal Structure of Kenoargentotetrahedrite-(Fe), $Ag_6Cu_4Fe_2Sb_4S_{12}$, from the Bajiazi Pb-Zn Deposit, Liaoning, China, Crystals, 12, 467, https://doi.org/10.3390/cryst12040467, 2022.

von Schnering, H. G. and Hoenle, W.: New compounds containing $Ag_6(^{4+})$ cluster units, Solid Compound of Transition Elements, Int. Conference Stuttgart, 12–16 June, 101–102, 1979.

von Weissenbach, C. G. A.: Ueber die Gehalte der beym sächsischen Bergbau vorkommenden Silbererze. Kalender für den Sächsischen Berg-und Hüttenmann auf das Jahr, 223–248, 1831.

Wang, Y., Chen, R., Gu, X., Nestola, F., Hou, Z., Yang, Z., Dong., G., Guo, H., and Qu, K.: Tetrahedrite-(Ni), $Cu_6(Cu_4Ni_2)Sb_4S_{13}$, the first nickel member of tetrahedrite group mineral from Luobusa chromite deposits, Tibet, China, Am. Min., 108, 1984–1992, 2023a.

Wang, Y., Chen, R., Gu, X., Hou, Z., Nestola, F., Yang, Z., Fan, G., Dong, G., and Qu, K.: Tennantite-(Ni), $Cu_6(Cu_4Ni_2)As_4S_{13}$, from Luobusa ophiolite, Tibet, China: a new Ni member of the tetrahedrite group, Mineral. Mag., 87, 591–598, 2023b.

Warr L. N.: IMA–CNMNC approved mineral symbols, Mineral. Mag., 85, 291–320, 2021.

Welch, M. D., Stanley, C. J., Spratt, J., and Mills, S. J.: Rozhdestvenskayaite $Ag_{10}Zn_2Sb_4S_{13}$ and argentotetrahedrite $Ag_6Cu_4(Fe^{2+}, Zn)_2Sb_4S_{13}$: two Ag dominant members of the tetrahedrite group, Eur. J. Mineral., 30, 1163–1172, 2018.

Wilson, A. J. C.: International Tables for Crystallography, Vol. C, Kluwer, Dordrecht, the Netherlands, eBook ISBN: 978-1-4020-5408-2, https://doi.org/10.1107/97809553602060000103, 1992.

Wu, P., Yang, H., Qu, K., Wang, Y., and Gu, X.: Argentotetrahedrite-(Hg) $Ag_6(Cu_4Hg_2)Sb_4S_{13}$: a new tetrahedrite group mineral from Dongping Hg-Ag deposit, Acta Geol. Sin., 96, 418–425, 2022 (in Chinese with English abstract).

Wuensch, B. J.: The crystal structure of tetrahedrite, $Cu_{12}Sb_4S_{13}$, Z. Kristallogr. Cryst. Mater., 119, 437–453, 1964.

Zhang, J., Chen, Y., Yang, Y., and Deng, J.: Lead isotope systematics of the Weishancheng Au-Ag belt, Tongbai Mountains, central China: implication for ore genesis, Int. Geol. Rev., 53, 656–676, 2011.

Zhang, J., Chen, Y. J., Pirajno, F., Deng, J., Chen, H. Y., and Wang, C. M.: Geology, C–H–O–S–Pb isotope systematics and geochronology of the Yindongpo gold deposit, Tongbai Mountains, central China: Implication for ore genesis, Ore Geol. Rev., 53, 343–356, 2013.

Zhdanov, Y. Y., Amuzinskiy, V. A., and Andrianov, N. G.: A natural variety of high-silver fahlerz with a large unit-cell parameter, Dokl. Akad., Earth Sci. Sect., 327, 134–138, 1992.